International Journal of Nanomedicine Dovepress

Open Access Full Text Article ORIGINAL RESEARCH

Self-Assembled EGCG Nanoparticles with Enhanced Intracellular ROS Scavenging for Skin Radioprotection

Xiaowen Han[1], Ruiling Xu[1], Yang Xia[2], Ying Liu[3], Shan Chen[3], Mingsong Shi[1], Zhiyan Zou[1], Yuanyuan Liang[1], Tingting Chen[1], Yufeng Tang[4], Wei Tang[3], Xiaoan Li[1,5], Liangxue Zhou[2,6,7]

[1]NHC Key Laboratory of Nuclear Technology Medical Transformation, Mianyang Central Hospital, School of Medicine, University of Electronic Science and Technology of China, Mianyang, 621000, People's Republic of China; [2]Department of Neurosurgery, Mianyang Central Hospital, School of Medicine, University of Electronic Science and Technology of China, Mianyang, 621000, People's Republic of China; [3]Institute of Materials, China Academy of Engineering Physics, Jiangyou, 621907, People's Republic of China; [4]Department of Neurology, Mianyang Central Hospital, School of Medicine, University of Electronic Science and Technology of China, Mianyang, 621000, People's Republic of China; [5]Department of Gastroenterology, Mianyang Central Hospital, School of Medicine, University of Electronic Science and Technology of China, Mianyang, 621000, People's Republic of China; [6]Department of Neurosurgery, West China Hospital, West China Medical School, Sichuan University, Chengdu, Sichuan, 610041, People's Republic of China; [7]Department of Neurosurgery, the Fifth People's Hospital of Ningxia, Shizuishan, Ningxia, 753000, People's Republic of China

Correspondence: Xiaoan Li; Liangxue Zhou, Mianyang Central Hospital, School of Medicine, University of Electronic Science and Technology of China, Mianyang, 621000, People's Republic of China, Email lixiaoan@sc-mch.cn; liangxue_zhou@126.com

Purpose: Skin radiation damage is a prevalent form of tissue injury encountered during radiotherapy, radiation accidents, and occupational exposure. The only clinically approved radioprotective agent, amifostine, is associated with numerous side effects, underscoring the urgent need for the development of safe and effective radioprotective agents. Natural products with reductive properties possess high antioxidant activity and biocompatibility, but their low bioavailability limits their radioprotective efficacy and clinical application. To address this, we utilized epigallocatechin gallate (EGCG) as a model compound and employed nanotechnology to enhance cellular uptake of natural compounds, thereby improving their free radical scavenging capabilities.

Methods: EGCG nanoparticles (EGCG NPs) with robust intracellular reactive oxygen species (ROS) scavenging ability were prepared via self-assembly. The morphology, size distribution, and antioxidant capacity of EGCG NPs were characterized. Cytocompatibility, intracellular ROS levels and DNA damage, cell migration and immune response of EGCG NPs to macrophages were tested in vitro. The in vivo radiation protection and biocompatibility of EGCG NPs were assessed in murine model.

Results: The EGCG NPs was successfully prepared and compared to free EGCG, EGCG NPs demonstrated better cellular uptake, significantly enhancing their biocompatibility, intracellular ROS scavenging capacity, and ability to mitigate DNA damage. Furthermore, EGCG NPs facilitated fibroblast proliferation and migration, while inhibiting the polarization of macrophages towards the M1 phenotype in vitro. In animal levels, EGCG NPs exhibited markedly improved radioprotective efficacy over free EGCG, effectively reducing skin edema and ulceration, alleviating pathological conditions such as interstitial edema, dermal fluid accumulation, and inflammatory infiltration, decreasing the duration of skin injury, and promoting wound healing.

Conclusion: This work offers novel insights into the therapeutic application of EGCG NPs as a potential alternative for skin radioprotection and provides a powerful approach for developing radioprotective agents derived from natural products.

Keywords: radiation-induced skin injury, nanoparticles, free radicals scavenging, radioprotection

Introduction

Radiation-Induced Skin Injury (RISI) is a prevalent complication observed in cancer patients undergoing radiotherapy (RT) and in cases of radiological accidents. As the first line of defense against external stimuli, the skin is highly susceptible to radiation damage, with over 95% of patients undergoing RT experience acute skin injuries, including dermatitis, erythema, alopecia, and ulceration.[1,2] Without timely and effective intervention, the damage to both local skin and deeper tissues can escalate, leading to recurrent infections and the transformation of acute wounds into chronic

Received: 2 September 2024
Accepted: 26 November 2024
Published: 6 December 2024

Graphical Abstract

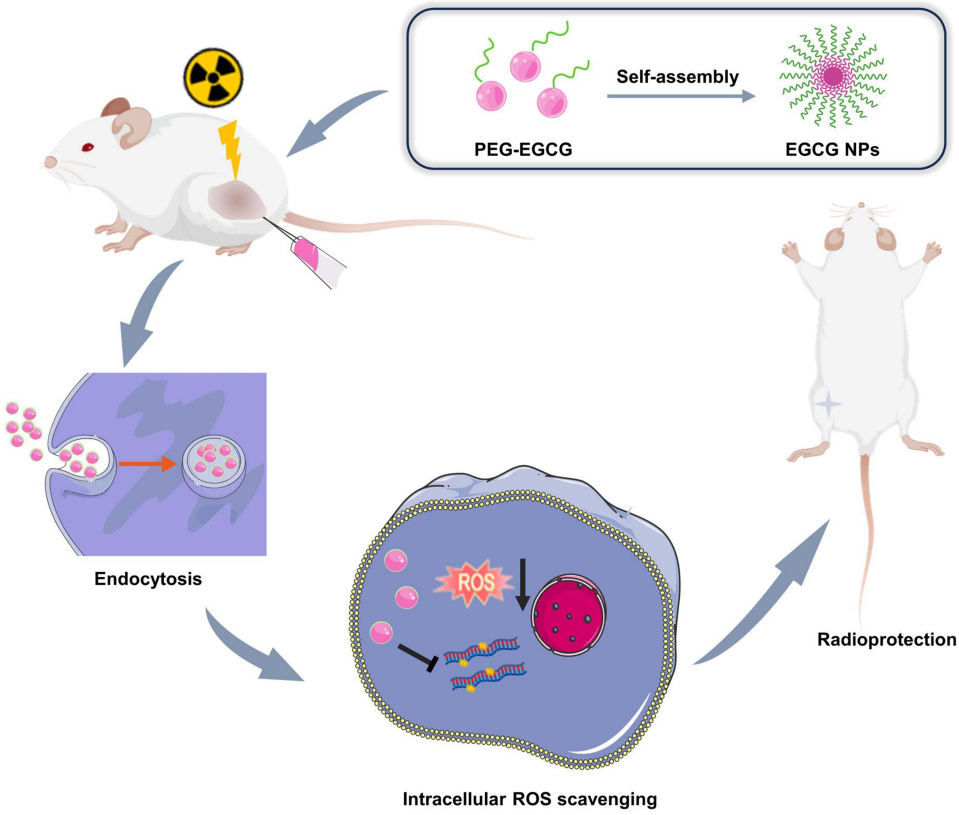

wounds.[3] This irreversible damage results in persistent wound healing issues, severely impacting the patient's quality of life. The early application of radioprotective drugs/material or interventions is crucial for diminishing the occurrence and progression of RISI. The specific pathological mechanisms underlying RISI remain incompletely elucidated, but may be attributed to direct DNA damage and reactive oxygen species (ROS) production.[4–6] ROS serve as a primary mechanism in radiation-induced injury, not only directly causing oxidative damage to cells but also potentially triggering inflammatory responses.[7–9] Therefore, the development of drugs/materials capable of scavenging ROS represents a principal research focus in the field of RISI prevention and repair.

To date, amifostine (WR-2721) remains the only approved radioprotective agent in clinical use. However, its clinical application is significantly constrained by severe adverse effects such as transient hypotension, nausea, and vomiting, as well as the necessity for intravenous administration.[10,11] In recent years, reductive natural compounds, such as epigallocatechin gallate (EGCG), curcumin and flavonoids, have been applied in preclinical and clinical studies for the protection against RISI.[12–14] These compounds play a critical role in mitigating radiation injury by interrupting the chain reaction of free radicals and donating hydrogen atoms to repair damaged molecules.[15] Despite their superiority, these natural compounds face challenges related to cellular uptake, which limits their effectiveness in scavenging intracellular ROS and diminishes their overall radioprotective effects[12,16.] Taken EGCG for instance, EGCG is a polyphenolic compound extracted from green tea, known for its ability to scavenge ROS and reduce oxidative damage. Previous studies have highlighted its potential in the prevention and treatment of skin injury.[17] Compared to other ROS-scavenging materials such as cerium oxide nanoparticles and amifostine, EGCG possesses excellent biocompatibility and the potential to modulate immune responses.[1] Nevertheless, its clinical application is hindered by issues such as poor stability, low

bioavailability, low cellular penetration, and rapid cellular efflux. Therefore, it is crucial to enhance the cellular uptake of EGCG and improve its bioavailability.

Nanoparticle technologies hold significant promise in transforming poorly absorbed, and unstable physiologically active compounds into viable therapeutic agents.[18,19] The small size of nanoparticles (NPs) allows them to traverse cellular membranes through gaps or via endocytosis mechanisms.[20–23] Moreover, the specific surface properties of nanoparticles play a crucial role in their bioactivity. For example, polyethylene glycol (PEG)-grafted nanoparticles have demonstrated enhanced stability and prolonged circulation time of drugs due to their high surface area.[24] Self-assembly technology facilitates the spontaneous organization of molecules into nanoparticles through non-covalent interactions such as hydrogen bonding, electrostatic interactions, and hydrophobic forces.[25–27] With its advantages of simplicity, cost-effectiveness, and strong controllability, self-assembly is widely used in nanoparticle preparation. Utilizing self-assembly techniques, it is possible to construct nanostructures with specific functions that can respond to changes in the cellular microenvironment, thereby enhancing cellular drug uptake.[28] Derivatives of EGCG, when utilized as drug delivery vectors, have been documented to augment the efficacy of drug delivery and to exert synergistic therapeutic effects.[29] However, investigations into their distinct biological impacts remain sparse. Therefore, we proposed that, converting free EGCG into nanoparticles through self-assembly technology could be an effective strategy to enhance its cellular endocytosis, improve bioavailability, and increase therapeutic efficacy.

In this study, we prepared PEG-modified EGCG, which subsequently self-assembled into EGCG nanoparticles (EGCG NPs). Compared to free EGCG, these EGCG NPs demonstrated preferable cellular uptake, significantly enhancing their biocompatibility, intracellular ROS scavenging capacity, and ability to mitigate DNA damage. Furthermore, EGCG NPs facilitated fibroblast proliferation and migration, while inhibiting the polarization of macrophages towards the M1 phenotype in vitro. In animal levels, EGCG NPs exhibited markedly improved radioprotective efficacy over free EGCG and amifostine, effectively reducing skin edema and ulceration, alleviating pathological conditions such as interstitial edema, dermal fluid accumulation, and inflammatory infiltration, decreasing the duration of skin injury, and promoting wound healing. This work not only unveils the potential application of EGCG NPs as radiation protectants but also introduces a novel approach for developing natural compounds for the protection and treatment of RISI.

Materials and Methods

Materials

PEG-SH (MW = 2 kDa) was provided by Shanghai yuanye Bio-Technology Co., Ltd. EGCG (98%) were obtained from Shanghai Macklin Biochemical Technology Co., Ltd. Analytical reagent of dimethyl sulfoxide (DMSO), acetic acid, and chloroform were purchased from Chengdu Kelong Chemical Co., Ltd. Amifostine (≥98%) was brought from Shanghai MedChemExpress Co., Ltd. PBS, cell counting kit-8 (CCK-8), DMEM medium, fetal bovine serum, simulated body fluid (SBF), penicillin-streptomycin and trypsin were provided by Gibco (USA). IL-4, TNF-α, IL-6 Elisa kit were purchased from Dakewei Biotech Co., Ltd. 4′,6-diamidino-2-phenylindole (DAPI), 2′,7′-Dichlorofluorescein diacetate (DCFH-DA), modified masson's trichrome stain kit, DPPH and ABTS free radical scavenging capacity assay kit, and lactate dehydrogenase (LDH) cell proliferation and toxicity detection kit were brought from Beijing Solarbio Science & Technology Co., Ltd. DNA damage assay kit by γ-H2AX immunofluorescence and paraformaldehyde were provided by Beyotime Biotechnology Co., Ltd. Gentian violet was purchased from Biosharp Technology Co., Ltd. All other chemicals were used without further purification.

Preparation and Characterization of PEG-EGCG

PEG-EGCG was synthesized according to a previous report with some modifications.[29] Briefly, 18.8 mg of EGCG was dissolved in a 20 mL mixture of PBS and DMSO with a volume ratio of 1:1, and PEG-SH was dissolved in PBS at a concentration of 5 mg/mL. The above solutions were mixed and stirred for 7 hours. Afterward, acetic acid was added to adjust the pH to 4.0, terminating the reaction. The PEG-EGCG solution was then transferred, dialyzed, and lyophilized

for 3 d. The lyophilized sample was tested by 1H-nuclear magnetic resonance spectra (1H-NMR, 400 MHz, Bruker AMX-400, USA).

Preparation and Characterization of EGCG NPs

PEG-EGCG was fully dissolved in chloroform and then subjected to rotary evaporation under reduced pressure for 1 hour (50 rpm) to remove the chloroform, forming a homogeneous thin film at the bottom of the flask. Deionized water was then added, and the mixture was incubated under nitrogen for 24 hours (in a 45°C water bath). Finally, the solution was passed through a 0.45 μm aqueous filter to remove unreacted free drug, and EGCG NPs was obtained. The morphology of EGCG NPs was observed by Transmission Electron Microscope (TEM, Tecnai G2 F20 S-TWIN, FEI, USA). A dynamic light scattering (DLS, ZetaSizer Nano, UK) was utilized to explore the size distribution and zeta potential of EGCG NPs. The stability of EGCG NPs in DMEM, PBS, and SBF was tested for a period of 7 days.

Antioxidant Capacity Test

DPPH Free Radicals Scavenging Assay

The DPPH free radicals scavenging ability of EGCG NPs was tested follow the manufacturer's instructions. Firstly, DPPH ethanol solution (100×10^6 mol/L), free EGCG and EGCG NPs solutions with different concentrations (10, 20, 30, 40, 50 and 60 μg/mL) were prepared. Then, 190 μL of DPPH ethanol solution was mixed with 10 μL of PBS/free EGCG/EGCG NPs solution. The mixed solutions were kept for 30 min in the dark. Finally, the absorption at 515 nm in different groups were measured and recorded. The free radicals scavenging efficiency of DPPH was calculated: (A1-(A2-A3))/A1, where, A1 is absorbance of DPPH, A2 is absorbance of DPPH and mixture, and A3 is absorbance of free EGCG/EGCG NPs solution.

ABTS Free Radicals Scavenging Assay

The ABTS free radicals scavenging assay is similar to the DPPH method. Briefly, the working solution of ABTS was prepared according to the manufacturer's instructions. Then, free EGCG and EGCG NPs solutions with different concentrations (10, 20, 30, 40, 50 and 60 μg/mL) were prepared. ABTS working solution was mixed with EGCG solutions/PBS afterwards. The mixed solutions were kept for 6 min in the dark. The absorbance of three paralleled wells at the wavelength of 405 nm were measured and recorded. Finally, the free radicals scavenging efficiency of ATBS was calculated: (A1-(A2-A3))/A1, where, A1 is absorbance of ABTS, A2 is absorbance of ABTS and mixture, and A3 is absorbance of free EGCG/EGCG NPs solution.

Cytotoxicity of EGCG NPs

Human immortalized keratinocytes (HaCaT cells, Cell Bank of the Chinese Academy of Sciences) were cultured in DMEM medium with 10% (v/v) FBS, and 1% penicillin-streptomycin at 37 °C and 5% CO_2. HaCaT cells were seeded in a 96-well plate at a density of 8×10^3 cells per well and incubated for 24 h, followed by a co-incubation of 48 h with free EGCG or EGCG NPs solutions with different concentrations (10, 20, 30, 40, 50, 60 μg/mL) respectively. Cells were seeded in a 96-well plate without EGCG solutions served as the positive control. At 24 h and 48 h, the culture medium was carefully removed and cell viability was evaluated by CCK-8 assay. The absorbance of three paralleled wells at the wavelength of 450 nm was measured and recorded. The cell viability was determined by: (A1-A0)/(A2-A0)×100%, where, A0 is absorbance of CCK8 solution, A1 is absorbance of samples, A2 is absorbance of positive control.

Radiation Protective Ability of EGCG NPs in vitro

Intracellular ROS Detection

HaCaT cells were cultured in confocal dishes at a density of 5×10^4 cells per dish, 24 h before radiation, the culture medium was replaced by free EGCG and EGCG NPs solutions respectively. Then, the mixture of DCFH-DA was employed to stain HaCaT for 30 min before removal. Next, cells were exposed to 6 Gy of X-ray radiation (X-Rad 320,

Precision Xray Inc., USA) at a fixed dose rate of 2 Gy/min. Finally, cells were observed by confocal laser scanning microscope (CLSM, Stellaris 5, Leica, Germany).

Intracellular DNA Damage Detection

HaCaT cells were grown in confocal dishes at a density of 5×10^4 cells per dish with culture medium. After incubated for 24 h, cells were cultured with free EGCG and EGCG NPs solutions for another 24 h. Then, HaCaT cells were exposed to 6 Gy of X-ray radiation at a fixed dose rate of 2 Gy/min. Cells were then fixed and stained with 4% paraformaldehyde and γH2AX/DAPI staining, respectively. Finally, CLSM was used to image the HaCaT cells.

Cell Viability After Radiation

HaCaT cells were seeded in a 24-well plate at a density of 1×10^5 cells per well with DMEM culture medium. Next, cells were subjected to 6 Gy of X-ray radiation at a dose rate of 2 Gy/min. After 12 h, the cell viability of HaCaT cells was evaluated by CCK-8 and LDH assay. The LDH assay was performed following the manufacturer protocol. Briefly, cells were lysed and collected. The absorbance of three paralleled samples at the wavelength of 490 nm was measured and recorded.

Cell Migration Ability

Scratch Assay

Mouse fibroblast cells (NIH/3T3 cells, American type culture collection) were used to assess the effect of EGCG NPs on cell migration. NIH/3T3 cells were cultured in a 24-well plate (1×10^5 cells/well) with DMEM medium containing 10% (v/v) FBS, and 1% penicillin-streptomycin. When cells are confluent, a straight scratch line was carefully made at the center of each well with a 200 μL tip. Detached cells were removed by PBS washing, and culture medium was replaced by DMEM medium containing free EGCG or EGCG NPs. Pictures of scratch lines were taken after culturing in conditioned media before and after 8 h. The migration areas were analyzed and measured using ImageJ software.

Transwell Assay

For transwell migration assay, NIH/3T3 cells exposed to 6 Gy of X-ray radiation were seeded in the upper chamber of 24-well Transwell plates at a density of 1×10^4 cells/well and cultured with DMEM medium. DMEM culture media with free EGCG or EGCG NPs were added to the lower chamber and then cultured for 24 h. Afterwards, cells in the upper chamber were fixed with 4% paraformaldehyde before they were stained with gentian violet. Photographs of migrated cells were taken and chambers were then soaked in a 33% acetic acid solution for decolorization for 1 h, and the absorbance of the decolorized solution was measured at 570 nm.

Immune Response of EGCG NPs to Macrophages in vitro

RAW264.7 cells (Cell Bank of the Chinese Academy of Sciences) were seeded on coverslips at a density of 1×10^4 cells/well and incubated with DMEM culture media containing free EGCG/EGCG NPs for 48 h. Then, coverslips were collected and washed twice with PBS before fixing with 4% paraformaldehyde. Cell culture supernatants were collected and stored at −80°C. Macrophage polarization and inflammatory cytokines secretion were detected through immunofluorescence staining and Elisa kit.

In vivo Radiation Protection of EGCG NPs

Twenty four Balb/c mice were randomly assigned to four groups (n=6) and given a subcutaneous injection of 100 μL of PBS/ amifostine/Free EGCG/EGCG NPs solution (25 mg/kg) in the thigh 1 h before irradiation. Then mice were subjected to X-ray (20 Gy) irradiation in the lower limb. The skin lesions of the mice were photographed on days 4, 7, and 14. On days 7 and 14, the skin tissues (n=3) were collected, fixed, paraffin embedded, sliced, and then stained with hematoxylin and eosin (H&E) and Masson's Trichrome Staining. All animal procedures have been approved by the guideline for Care and Use of Laboratory Animals Ethical Committee at Mianyang Central Hospital and were following the guideline for ethical review of laboratory animal welfare (GB/T 35872–2018).

Biosafety of EGCG NPs

For biosafety of EGCG NPs, nine Balb/c mice were randomly divided into three groups (n=3): (1) Control, (2) Free EGCG and (3) EGCG NPs. Group (2) and (3) were given 100 μL of EGCG/EGCG NPs solution (25 mg/kg) respectively, while Group (1) was given 100 μL of PBS. On days 14, blood samples of mice were collected for biochemical analysis, and major organs (heart, liver, spleen, kidney, lungs) were collected for tissue embedding, sectioning, and H&E staining.

Statistical Analysis

All data were presented as mean ± standard deviation (SD) of at least three representative experiments. SPSS 22.0 software was used for statistical analysis using one-way ANOVA. The difference was statistically significant at three levels. *$P<0.05$, **$P<0.01$, and ***$P<0.001$.

Results and Discussion

Characterization and Cellular Uptake of EGGC NPs

First, thiolated polyethylene glycol (PEG-SH) was modified onto the EGCG to fabricate PEG-EGCG, and its molecular structures was confirmed by 1H-NMR (Figure S1). Then, PEG-EGCG was fully dissolved in chloroform to form EGCG NPs via self-assembly technology, as shown in Figure 1A. Transmission electron microscopy (TEM) images and dynamic light scattering (DLS) spectroscopy showed that the EGCG NPs was spherical, with a particle size of around 150 nm, zeta potential of −16 mV (Figure 1B, and S2). Additionally, the hydrodynamic size variation of EGCG NPs in various media was monitored over a prolonged incubation time up to 7 days, where their size did not show notable enlargement until day 7 (Figure 1C). EGCG has a strong free radical scavenging ability that is widely used as antioxidant.[30] Therefore, the DPPH and ABTS free radical scavenging ability of EGCG NPs were evaluated (Figure 1D). It could be observed that, with the exception of the 10 μg/mL concentration, the DPPH and ABTS free radical scavenging ability of free EGCG are higher than that of EGCG NPs at other concentrations (10–60 μg/mL). This discrepancy may be attributed to the partial oxidation of hydroxyl groups of EGCG during the synthesis process. However, EGCG NPs exhibited favorable biocompatibility, showing no cytotoxicity even at high concentrations (60 μg/mL). Furthermore, within the concentration range of 10–60 μg/mL, the cellular viability associated with EGCG NPs was consistently higher than that observed with free EGCG at equivalent concentrations (Figure 1E). To investigate the cellular uptake capacity of EGCG NPs, they were labeled with the cell tracer, Dil, and co-cultured with HaCaT cells for 8 h, followed by observation under confocal laser scanning microscopy (CLSM). As shown in Figure 1F, EGCG NPs were endocytosed by the cells, with a colocalization coefficient reaching 0.97. These results demonstrated that EGCG NPs could be effectively endocytosed by cells, and exhibited excellent biocompatibility.

The Radiation Protective Ability of EGCG NPs in vitro

As previously mentioned, DNA damage and excessive ROS are critical factors in RISI.[6,31] Therefore, we subsequently examined the ability of EGCG NPs to reduce intracellular ROS levels and DNA damage. In Figure 2A, compared the RT group, cells treated with EGCG exhibited a significant reduction in intracellular ROS levels, with the EGCG NPs group demonstrating the lowest ROS levels. Immunofluorescent staining of γH2AX was applied to represent DNA double-strand breaks post-irradiation, it could be observed from the CLSM images and 3D reconstructed structures in Figure 2B1 and B2 that EGCG NPs significantly mitigated intracellular DNA double-strand breaks, indicating their potential in reducing irradiation-induced cellular damage. As a result, EGCG NPs could effectively protect DNA from ROS attack, reduce radiation induced oxidative stress and ultimately inhibit the cell apoptosis (Figure 2C).

Effect of EGCG NPs on Cell Migration and Macrophages Polarization

In radiation-induced wounds, cellular functions are compromised, manifesting as reduced proliferation and migration capabilities, leading to inadequate adhesion of cells, which in turn prolongs the wound healing process.[32] Thus, we next evaluated the cell proliferation promoting ability of EGCG NPs. NIH/3T3 cells were co-cultured with drugs and their proliferation capacity was assessed using the CCK-8 assay. As shown in Figure S3, after one day of

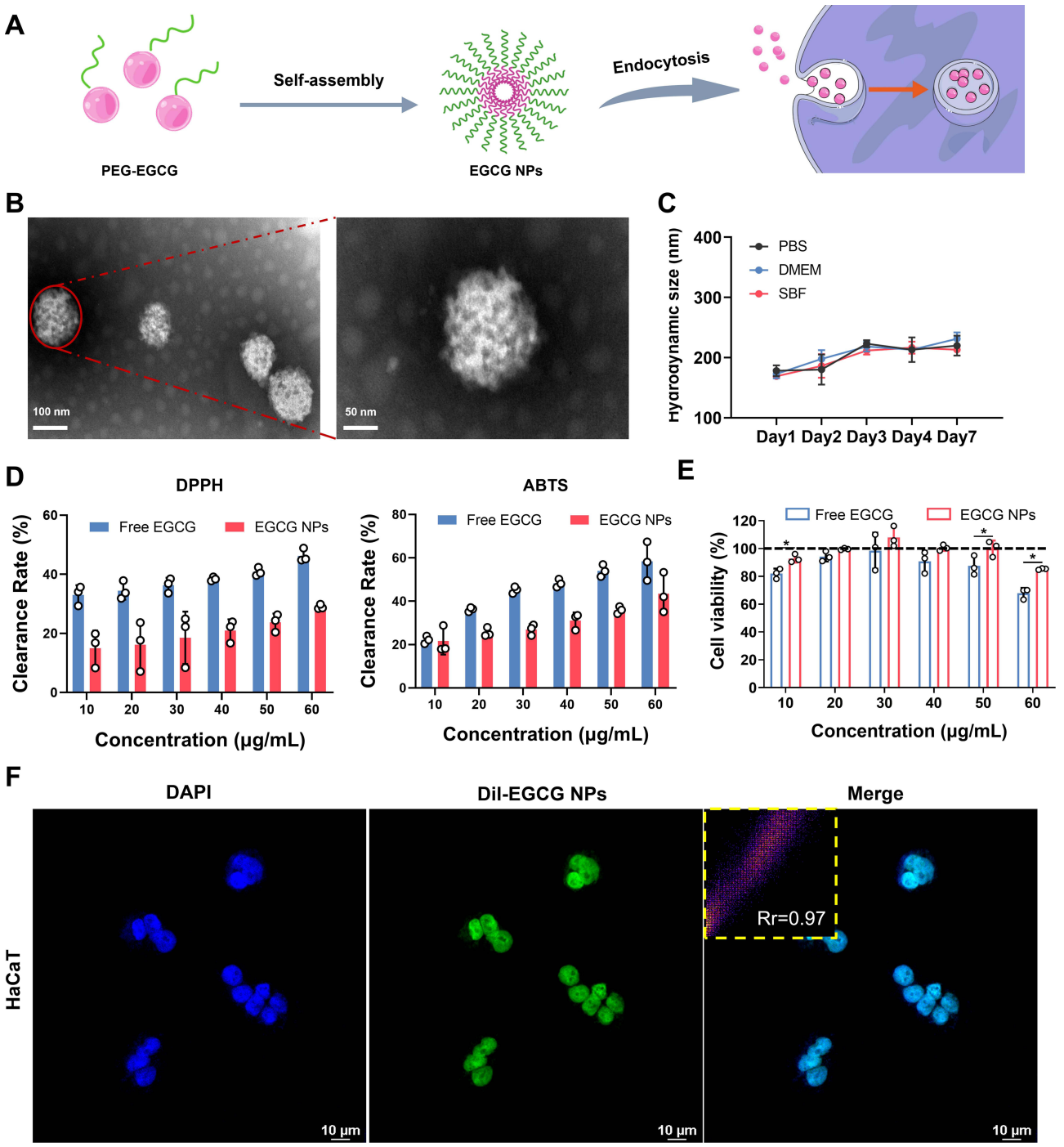

Figure 1 The preparation and characterization of EGCG NPs. (**A**) Schematic diagram of EGCG NPs fabrication. (**B**) TEM images and (**C**) stability of EGCG NPs. (**D**) DPPH and ABTS scavenging ability of EGCG NPs. (**E**) Cell viability of Free EGCG and EGCG NPs at different concentrations. (**F**) CLSM images for cellular uptake of EGCG NPs (scale bar: 10 μm). Significance levels of $*p<0.05$ were applied.

culture, the OD values of the fibroblasts in the EGCG NPs group were significantly higher than those in the other two groups, indicating an enhanced capacity for promoting cell proliferation. On day 3, both the Free EGCG and EGCG NPs groups exhibited higher OD values than the Control group, with the EGCG NPs group showing the highest OD values. This finding suggested that the nanoparticle form of EGCG more effectively promoted cell proliferation compared to free EGCG, likely due to its improved cellular uptake. Then, transwell and scratch assays

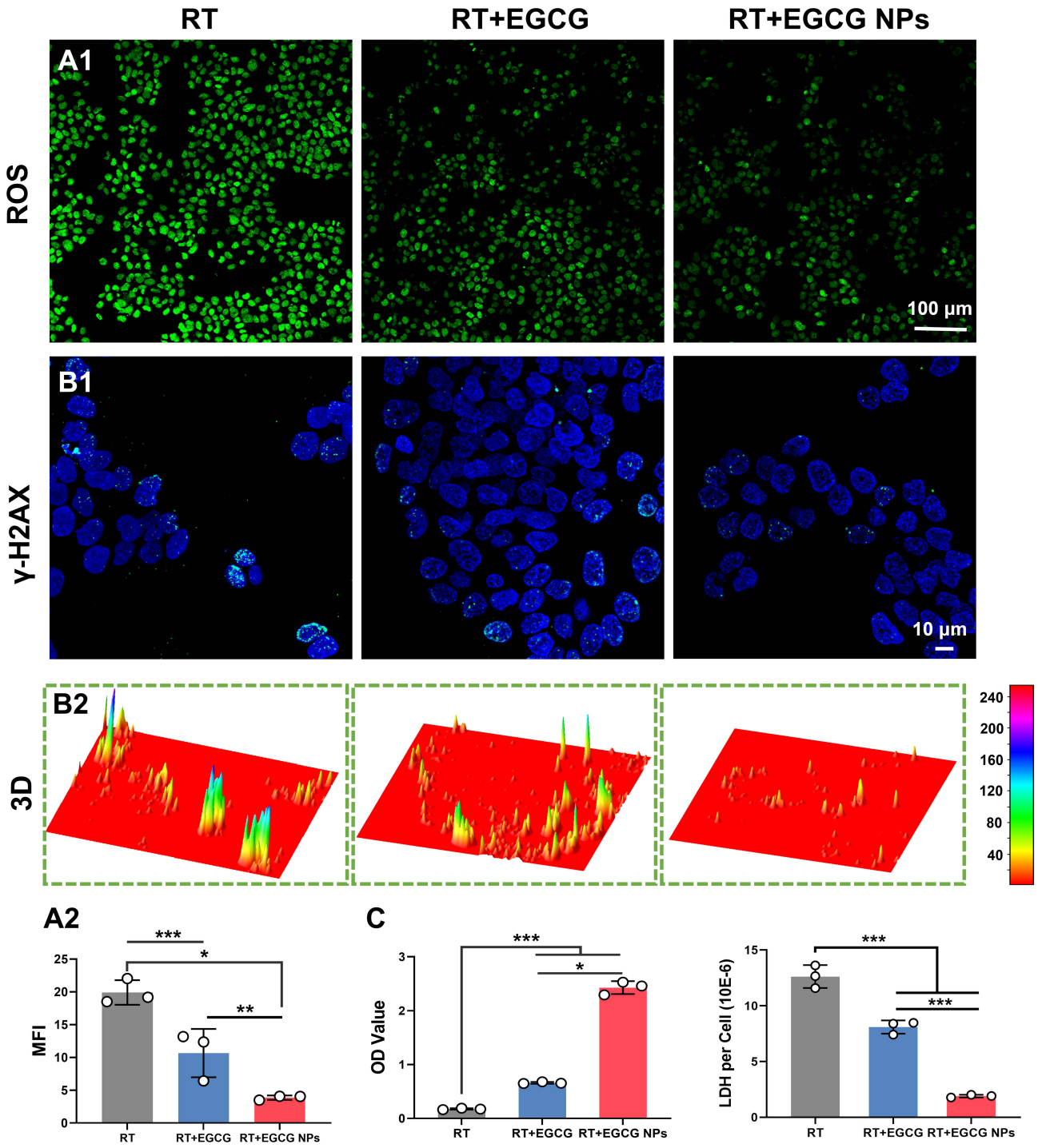

Figure 2 Radioprotection effect of EGCG NPs in vitro. (**A1**) Representative CLSM images of intracellular ROS level of HaCaT cells after radiation (scale bar: 100 μm) and (**A2**) corresponding mean fluorescence intensity of DCFH-DA staining (n=3). (**B1**) Immunofluorescence images of γ-H2AX representing DNA double-strand damage after different treatments (scale bar: 10 μm) and (**B2**) 3D reconstruction of γ-H2AX fluorescence by image J. (**C**) CCK-8 and LDH assay for HaCaT cells after radiation. Significance levels of *p<0.05, **p<0.01 and ***p<0.001 were applied.

were employed to investigate the impact of EGCG NPs on cellular migration capabilities. As shown in Figure 3A, after 24 h of co-culture, the control group exhibited only minimal cellular migration. In contrast, the Free EGCG and EGCG NPs groups demonstrated a significant increase in cellular migration compared to the control group.

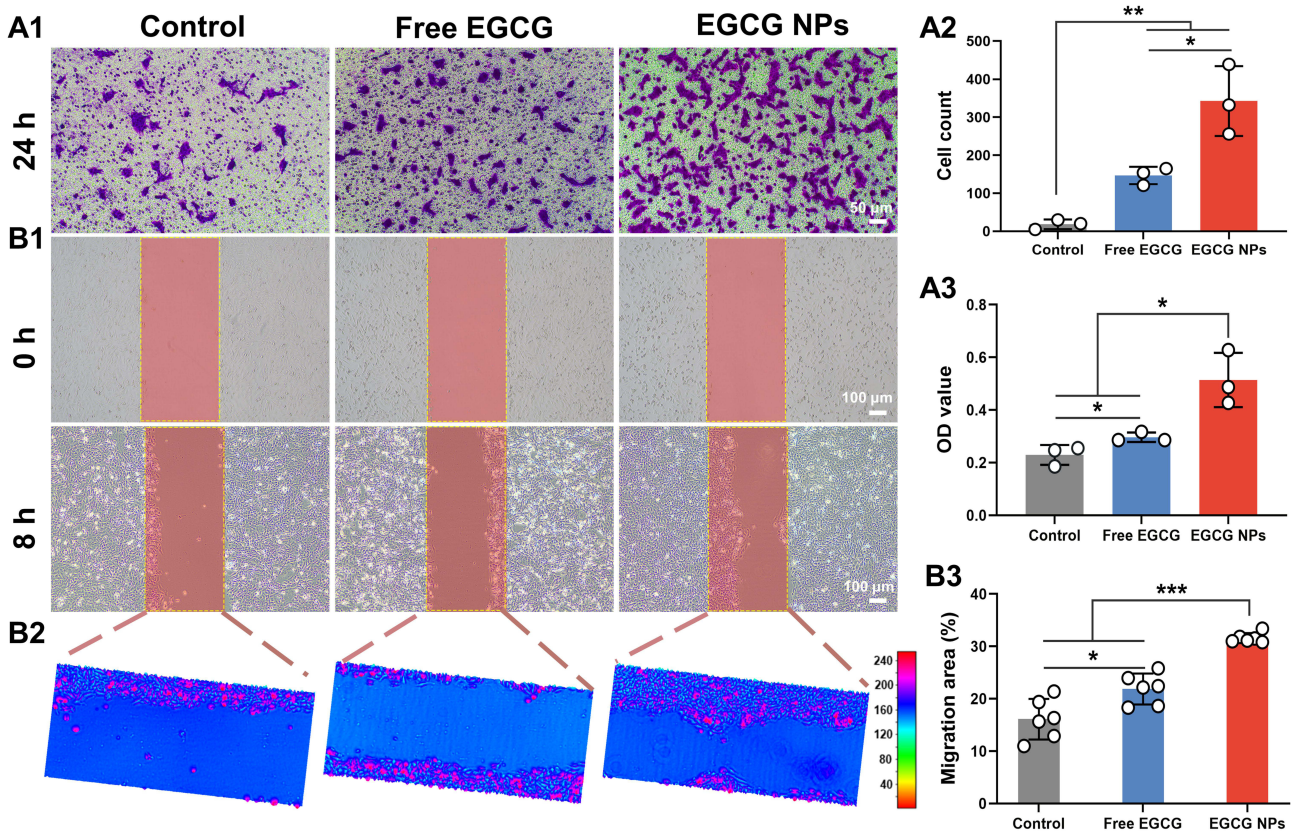

Figure 3 The effect of EGCG NPs on cell migration. (**A1**) Transwell assay of NIH/3T3 cells after incubation with drugs for 24 h (scale bar: 50 μm). (**A2**) Quantification of cell numbers by Image J and (**A3**) corresponding OD value of crystal violet staining. (**B1**) Scratch images of NIH/3T3 cells after incubation with drugs for 8 h (scale bar: 100 μm) and (**B2**) corresponding 3D reconstruction images. (**B3**) Quantitative analysis of migration area (n=6). Significance levels of **p*<0.05, ***p*<0.01 and ****p*<0.001 were applied.

Furthermore, cells in the EGCG NPs group fully spread and interconnected. Semi-quantitative results (Figure 3A2) revealed that the number of cells traversing the transwell chambers in the EGCG NPs group was markedly higher than in the other two groups, approximately 2.3 times that of the Free EGCG group. The OD values were also significantly higher in the EGCG NPs group, consistent with the cell count results (Figure 3A3). The closed scratch wound rate was used to assess the migration ability of cells after 8 h of treatment. As depicted in the intuitive images and 3D surface plots in Figure 3B1 and B2, the EGCG NPs group demonstrated a significantly enhanced repair effect compared to the larger non-healing areas observed in the control and Free EGCG groups. Statistical analysis of the closed wound rate (Figure 3B3) indicated that the healing area exceeded 30% showing a significant difference ($p < 0.05$) when compared to the control group (16.1 ± 3.89%) and the Free EGCG group (21.88 ± 2.95%). These results indicated that EGCG NPs could be endocytosed via endocytosis, reducing intracellular oxidative stress and promoting cellular migration.

Macrophages play a vital role in inflammation regulation and exert a profound influence on the process of RISI repair.[33] Macrophages can be categorized into the classical M1 and alternative M2 phenotypes, extensive research has demonstrated the crucial role of macrophages polarization in tissue repair.[34] Studies have shown the anti-inflammatory effects of EGCG, yet further exploration is needed to determine whether EGCG NPs can modulate macrophage phenotype switching.[35] Raw264.7 cells were co-cultured with EGCG NPs for 48 h, and subsequently subjected to immunofluorescence staining to evaluate their phenotype (Figure 4A). It could be observed that macrophages in the Control and Free EGCG groups exhibited abundant expression of CD86 fluorescence, whereas the EGCG NPs group showed a significant reduction in $CD86^+$ macrophages, indicating its ability to diminish M1 macrophage polarization.

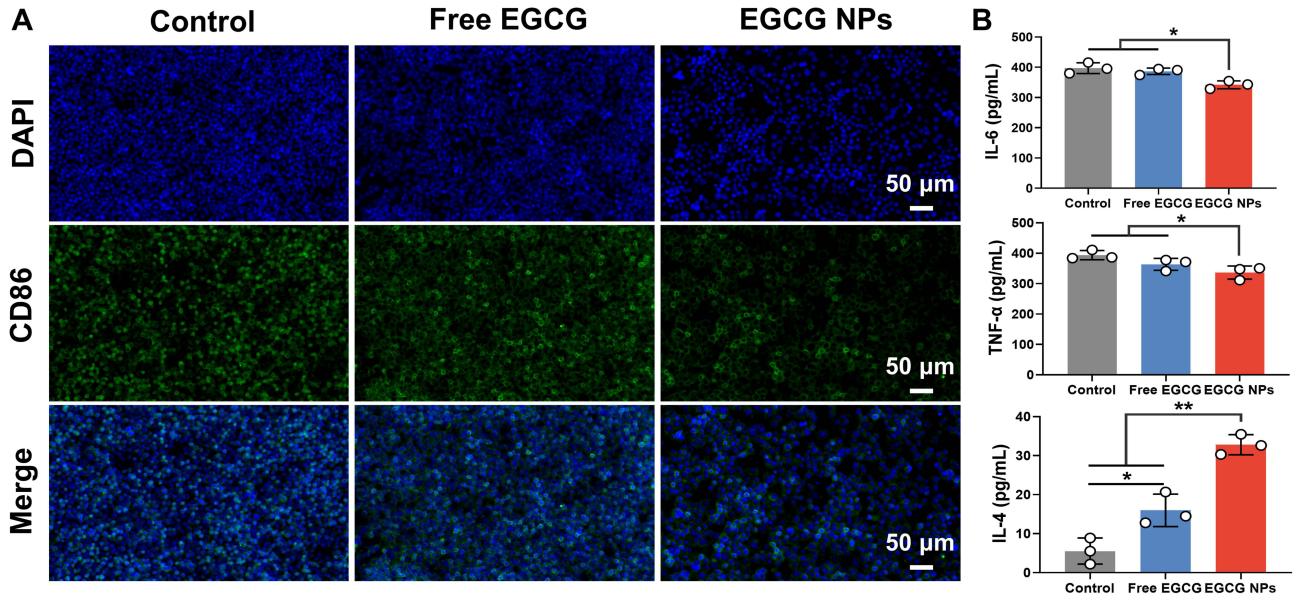

Figure 4 Macrophage polarization in vitro. (**A**) Immunofluorescence images of $CD86^+$ macrophages after incubation with drugs for 48 h (scale bar: 50 μm). (**B**) TNF-α, IL-6, and IL-4 concentrations in cell supernatant. Significance levels of *$p<0.05$ and **$p<0.01$ were applied.

Simultaneously, supernatants from the cultured macrophage groups were collected and subjected to ELISA for quantitative detection of inflammatory cytokines (Figure 4B). Compared to the other two groups, macrophages in the EGCG NPs group exhibited reduced secretion of pro-inflammatory factors (TNF-α and IL-6) and increased expression of anti-inflammatory factors (IL-4), potentially associated with the decreased proportion of M1-type macrophages. This suggested that EGCG NPs possessed anti-inflammatory properties, capable of providing a favorable microenvironment for wound repair and facilitating the recovery of RISI.

In vivo Radiation Protection of EGCG NPs

Inspired by the promising radioprotective outcomes observed in vitro, we proceeded to evaluate the in vivo radioprotective effect of EGCG NPs on the skin by visually monitoring changes in irradiated skin wounds in BALB/c mice and examining their corresponding histopathological phenomena. Figure 5A visually illustrated the skin wound alterations in mice subjected to various treatments prior to 20 Gy X-ray irradiation. On the 4th day, all groups exhibited obvious erythema, with the control group also presenting edema. By the 7th day, the wounds in the control and amifostine group had further deteriorated, showing ulceration and desquamation. The Free EGCG group developed dry desquamation and minor ulceration. In contrast, the EGCG NPs group showed significantly better wound conditions compared to the other three groups, displaying only slight desquamation without any ulceration. After 14 days, the wounds in the control group exhibited moist desquamation and unhealed ulcers. The amifostine and Free EGCG group showed moderate edema and desquamation, while the EGCG NPs group displayed substantial reduction in redness and swelling, with only minimal pigmentation. The pathological analysis was performed via H&E and Masson staining (Figure 5B). It could be observed that on the 7th day, the epidermal integrity in the control group was compromised, with a substantial accumulation of inflammatory cells at the defect site. The amifostine and Free EGCG group maintained better epidermal integrity compared to the control group, while the EGCG NPs group exhibited completely intact epidermis and the lowest degree of epithelial keratosis. On the 14th day, the control and amifostine group exhibited excessive hyperkeratosis in the epidermis layer, with a substantial infiltration of inflammatory cells in the dermis. The collagen fibers were arranged linearly, indicating a tendency to form linear scars.[36] In the Free EGCG group, the hyperkeratosis was relieved, with a significant deposition of collagen in the dermis, albeit with a more random orientation. In the EGCG NPs group, the epidermis was intact and comparable in thickness to uninjured tissue, with

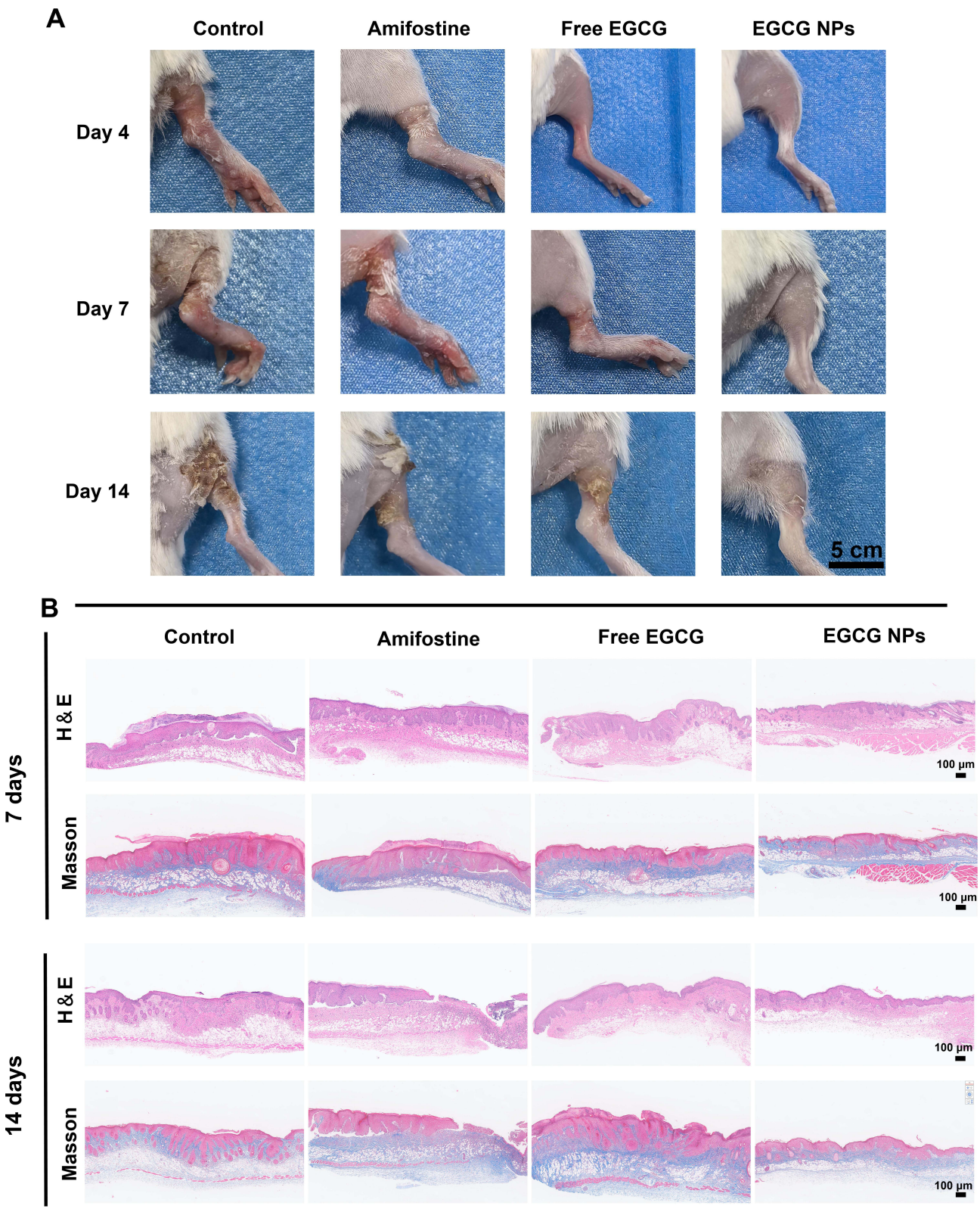

Figure 5 Radioprotective effect of EGCG NPs in vivo. (**A**) The photos of the skin wound changes of mice 0, 4, 7, 14 days after radiation. (**B**) The histopathology analysis of skin tissue after radiation for 7 and 14 days by H&E and Masson staining (scale bar: 100 μm).

newly formed collagen showing a random orientation and accompanying hair follicle regeneration. Based on these findings, it was evident that the EGCG NPs could partial protection to the skin against radiation-induced damage, which may attribute to the prominent intracellular ROS scavenging and anti-inflammatory capabilities of EGCG NPs, enabling them to reduce DNA damage and promote cellular migration.

Biosafety of EGCG NPs

Ensuring the biological safety of EGCG NPs is essential for its application in vivo for skin radioprotection. We thus administered subcutaneous injections of EGCG NPs in mice to assess their biological safety. After 14 days of treatment, major organs (heart, liver, spleen, lungs, and kidneys) were collected from the mice for H&E staining, and blood samples were collected for biochemical testing. From Figure 6A, it was obvious that the morphological structure of the heart, liver, spleen, lungs, and kidneys in the EGCG NPs group mice was not significantly different from that of the control group, indicating that there were no apparent toxic effects on the organ tissues of mice after administration. The results of the blood biochemical tests indicated that the hepatic function (ALT, AST, ALB), renal function (BUN, UA), and blood

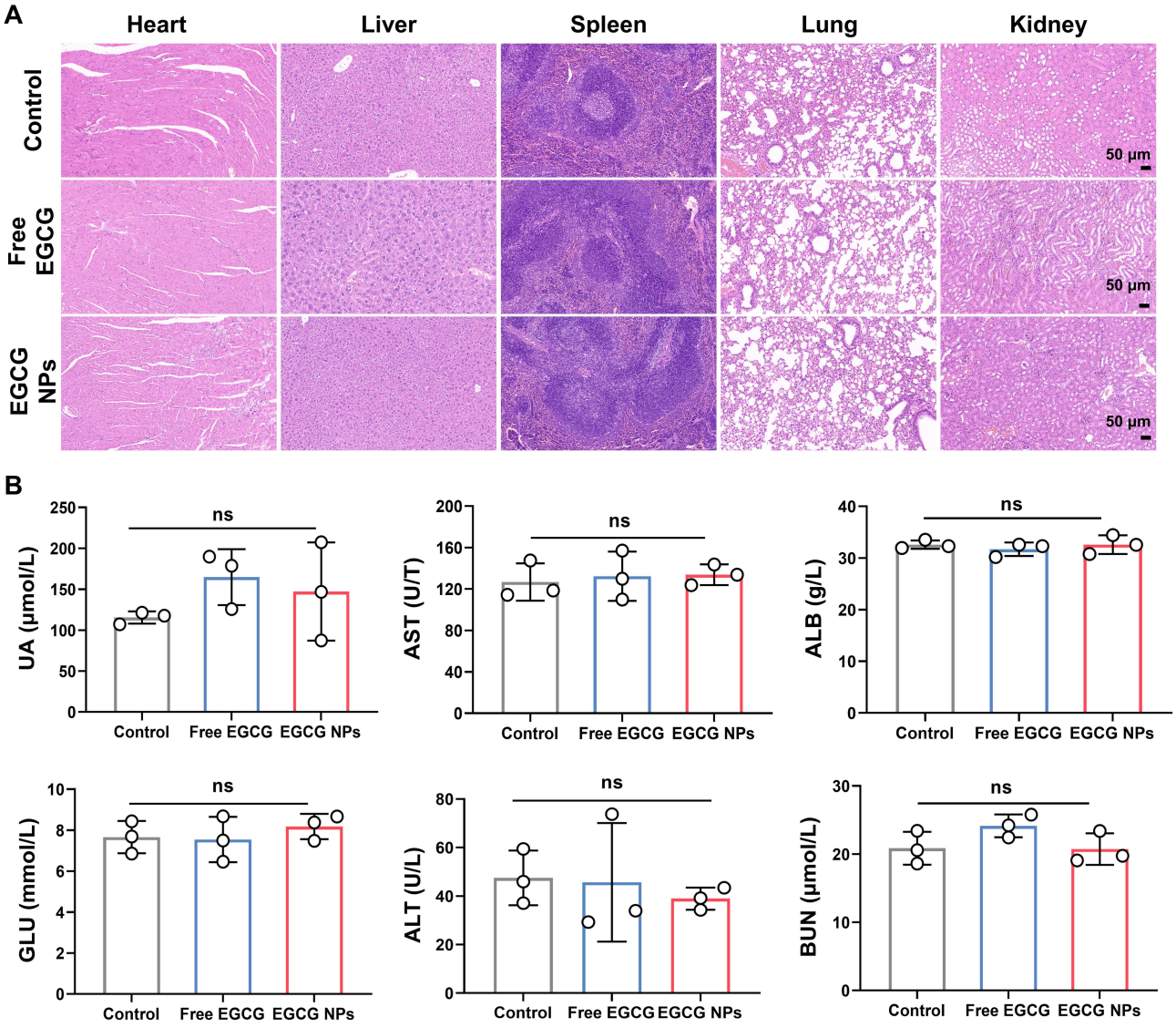

Figure 6 Biosafety of EGCG NPs. (**A**) H&E staining of heart, liver, spleen, lung, kidney of mice after subcutaneous injections of different drugs (scale bar: 50 μm). (**B**) The blood biochemistry data of mice after subcutaneous injections of different drugs (n=3).

glucose levels (GlU) in mice treated with EGCG NPs were within normal ranges and showed no significant differences compared to the Control group mice, which confirmed their biological safety.

Conclusion

In summary, to overcome the bottleneck of low bioavailability that limits the radioprotective efficacy of natural compounds, we utilized a self-assembly strategy to fabricate EGCG NPs. Compared to their free form, EGCG NPs exhibited excellent biocompatibility. More importantly, EGCG NPs was efficiently endocytosed into cells, significantly enhancing their intracellular ROS scavenging capabilities and thereby reducing radiation-induced DNA damage. Leveraging their favorable antioxidant and anti-inflammatory properties, EGCG NPs promoted the proliferation and migration of skin cells and exhibited immunomodulatory effects in vitro, reducing the M1 polarization of macrophages and lowering the expression levels of pro-inflammatory factors. In the animal model, the EGCG NPs effectively reduced edema, erythema, and ulcers induced by X-ray radiation in mice. It performed better than commercial radioprotector, amifostine, mitigated pathological lesions such as interstitial edema, hyperkeratosis, and inflammatory infiltration, and reduced the severity and duration of skin damage, thereby facilitating skin recovery. Moreover, EGGC NPs exhibited no apparent toxic side effect in vivo, demonstrating excellent biosafety. Our study demonstrated the potential application of EGCG NPs as radiation protectants, offering a novel strategy for the development of skin radioprotective agents derived from natural compounds. In future research, the radioprotective mechanism of EGCG NPs, such as its immune regulation effect, should be further considered and studied.

Acknowledgments

The Graphical Abstract was created in BioRender. Liu, H. (2024) https://BioRender.com/d30p749.

Funding

This work was sponsored by NHC Key Laboratory of Nuclear Technology Medical Transformation (MIANYANG CENTRAL HOSPTICAL, grant number 2023HYX014), Talent Introduction Project of Mianyang Central Hospital (grant number 2024RCGJ-002), Sichuan Science and Technology Program (grant number 2023YFS0470), Mianyang Science and Technology Bureau (Minyang Science and Technology Program, Grant NO. 2023ZYDF097).

Disclosure

The author(s) report no conflicts of interest in this work.

References

1. Wang Y, Yang L, Liu B, et al. Radiation Skin Injury Care in Radiotherapy for Oncology: mechanisms, Drug Therapy and Novel Biomaterial Application Strategies. *Adv Ther*. 2023;6(11):2300024. doi:10.1002/adtp.202300024.
2. Jaschke W, Schmuth M, Trianni A, Bartal G. Radiation-Induced Skin Injuries to Patients: what the Interventional Radiologist Needs to Know. *Cardiovasc Intervent Radiol*. 2017;40(8):1131–1140. doi:10.1007/s00270-017-1674-5
3. Wang Z, Chen Z, Jiang Z, et al. Cordycepin prevents radiation ulcer by inhibiting cell senescence via NRF2 and AMPK in rodents. *Nat Commun*. 2019;10(1):2538. doi:10.1038/s41467-019-10386-8
4. Wei J, Meng L, Hou X, et al. Radiation-induced skin reactions: mechanism and treatment. *Cancer Manag Res*. 2018;11:167–177. doi:10.2147/CMAR.S188655
5. Rosenthal A, Israilevich R, Moy R. Management of acute radiation dermatitis: a review of the literature and proposal for treatment algorithm. *J Am Acad Dermatol*. 2019;81(2):558–567. doi:10.1016/j.jaad.2019.02.047
6. Yang X, Ren H, Guo X, et al. Radiation-induced skin injury: pathogenesis, treatment, and management. *Aging*. 2020;12(22):23379. doi:10.18632/aging.103932
7. Wang Y, Tu W, Tang Y, Zhang S. Prevention and treatment for radiation-induced skin injury during radiotherapy. *Radiat Med Prot*. 2020;1(2):60–68. doi:10.1016/j.radmp.2020.02.004
8. Liu J, Han X, Zhang T, et al. Reactive oxygen species (ROS) scavenging biomaterials for anti-inflammatory diseases: from mechanism to therapy. *J Hematol Oncol*. 2023;16(1). doi:10.1186/s13045-023-01512-7.
9. Morris G, Gevezova M, Sarafian V, Maes M. Redox regulation of the immune response. *Cell Mol Immunol*. 2022;19(10):1079–1101. doi:10.1038/s41423-022-00902-0
10. Ji L, Cui P, Zhou S, et al. Advances of Amifostine in Radiation Protection: administration and Delivery. *Mol Pharm*. 2023;20(11):5383–5395. doi:10.1021/acs.molpharmaceut.3c00600

11. Zhang D, Zhong D, Ouyang J, et al. Microalgae-based oral microcarriers for gut microbiota homeostasis and intestinal protection in cancer radiotherapy. *Nat Commun*. 2022;13(1):1413. doi:10.1038/s41467-022-28744-4
12. Gan RY, Li HB, Sui ZQ, Corke H. Absorption, metabolism, anti-cancer effect and molecular targets of epigallocatechin gallate (EGCG): an updated review. *Crit Rev Food Sci Nutr*. 2018;58(6):924–941. doi:10.1080/10408398.2016.1231168
13. Verma A, Zanoletti A, Kareem KY, et al. Skin protection from solar ultraviolet radiation using natural compounds: a review. *Environ Chem Lett*. 2024;22(1):273–295. doi:10.1007/s10311-023-01649-4
14. Xie J, Yong Y, Dong X, et al. Therapeutic Nanoparticles Based on Curcumin and Bamboo Charcoal Nanoparticles for Chemo-Photothermal Synergistic Treatment of Cancer and Radioprotection of Normal Cells. *ACS Appl Mater Interfaces*. 2017;9(16):14281–14291. doi:10.1021/acsami.7b02622
15. Chen T, Zhuang B, Huang Y, et al. Inhaled curcumin mesoporous polydopamine nanoparticles against radiation pneumonitis. *Acta Pharm Sin B*. 2022;12(5):2522–2532. doi:10.1016/j.apsb.2021.10.027
16. Man J, Shen Y, Song Y, et al. Biomaterials-mediated radiation-induced diseases treatment and radiation protection. *J Control Release*. 2024;370:318–338. doi:10.1016/j.jconrel.2024.04.044
17. Wu Y, Wang Y, Zheng C, et al. A Versatile Glycopeptide Hydrogel Promotes Chronic Refractory Wound Healing Through Bacterial Elimination, Sustained Oxygenation, Immunoregulation, and Neovascularization. *Adv Funct Mater*. 2023;33(49):2305992. doi:10.1002/adfm.202305992
18. Yang B, Chen Y, Shi J. Reactive Oxygen Species (ROS)-Based Nanomedicine. *Chem Rev*. 2019;119(8):4881–4985. doi:10.1021/acs.chemrev.8b00626
19. Liu YX, Wu N. Progress of nanotechnology in diabetic retinopathy treatment. *Int J Nanomed*. 2021;16:1391–1403. doi:10.2147/IJN.S294807
20. Rennick JJ, Johnston APR, Parton RG. Key principles and methods for studying the endocytosis of biological and nanoparticle therapeutics. *Nat Nanotechnol*. 2021;16(3):266–276. doi:10.1038/s41565-021-00858-8
21. Cong VT, Houng JL, Kavallaris M, et al. How can we use the endocytosis pathways to design nanoparticle drug-delivery vehicles to target cancer cells over healthy cells? *Chem Soc Rev*. 2022;51(17):7531–7559. doi:10.1039/D1CS00707F
22. Zhang S, Gao H, Bao G. Physical Principles of Nanoparticle Cellular Endocytosis. *ACS Nano*. 2015;9(9):8655–8671. doi:10.1021/acsnano.5b03184
23. Ning J, Zheng G, Cai Y. The self-assembly soluplus nanomicelles of nobiletin in aqueous medium based on solid dispersion and their increased hepatoprotective effect on APAP-induced acute liver injury. *Int J Nanomed*. 2023;18:5119–5140. doi:10.2147/IJN.S426703
24. Suk JS, Xu Q, Kim N, et al. PEGylation as a strategy for improving nanoparticle-based drug and gene delivery. *Adv Drug Deliv Rev*. 2016;99:28–51. doi:10.1016/j.addr.2015.09.012
25. Tan SF, Raj S, Bisht G, et al. Nanoparticle Interactions Guided by Shape-Dependent Hydrophobic Forces. *Adv Mater*. 2018;30(16). doi:10.1002/adma.201707077.
26. Zhu K, Mu Y, Zhang M, et al. Mixed matrix membranes decorated with in situ self-assembled polymeric nanoparticles driven by electrostatic interaction. *J Mater Chem a Mater*. 2018;6(17):7859–7870. doi:10.1039/C8TA00317C
27. He H, Shen X, Nie Z. Engineering interactions between nanoparticles using polymers. *Prog Polym Sci*. 2023;143:101710. doi:10.1016/j.progpolymsci.2023.101710
28. Liang C, Yan X, Zhang R, et al. Enhanced cellular uptake and nuclear accumulation of drug-peptide nanomedicines prepared by enzyme-instructed self-assembly. *J Control Release*. 2020;317:109–117. doi:10.1016/j.jconrel.2019.11.028
29. Liang K, Chung JE, Gao SJ, et al. Highly Augmented Drug Loading and Stability of Micellar Nanocomplexes Composed of Doxorubicin and Poly (ethylene glycol)–Green Tea Catechin Conjugate for Cancer Therapy. *Adv Mater*. 2018;30(14). doi:10.1002/adma.201706963.
30. Nikoo M, Regenstein JM, Ahmadi Gavlighi H. Antioxidant and Antimicrobial Activities of (-)-Epigallocatechin-3-gallate (EGCG) and its Potential to Preserve the Quality and Safety of Foods. *Comprehensive Reviews in Food Science and Food Safety*. 2018;17:732–753. doi:10.1111/1541-4337.12346
31. Yang L, Ran H, Yin Y, et al. Mitochondrial targeted cerium oxide nanoclusters for radiation protection and promoting hematopoiesis. *Int J Nanomed*. 2024;19:6463–6483. doi:10.2147/IJN.S459607
32. Feng Z, Zhang Y, Yang C, et al. Bioinspired and Inflammation-Modulatory Glycopeptide Hydrogels for Radiation-Induced Chronic Skin Injury Repair. *Adv Healthc Mater*. 2023;12(1). doi:10.1002/adhm.202201671.
33. Meziani L, Deutsch E, Mondini M. Macrophages in radiation injury: a new therapeutic target. *Oncoimmunology*. 2018;7(10):e1494488. doi:10.1080/2162402X.2018.1494488
34. Murray PJ. On macrophage diversity and inflammatory metabolic timers. *Nat Rev Immunol*. 2020;20(2):89–90. doi:10.1038/s41577-019-0260-2
35. Nie R, Zhang QY, Tan J, et al. EGCG modified small intestine submucosa promotes wound healing through immunomodulation. *Compos B Eng*. 2023;267:111005. doi:10.1016/j.compositesb.2023.111005
36. Guo R, Merkel AR, Sterling JA, Davidson JM, Guelcher SA. Substrate modulus of 3D-printed scaffolds regulates the regenerative response in subcutaneous implants through the macrophage phenotype and Wnt signaling. *Biomaterials*. 2015;73:85–95. doi:10.1016/j.biomaterials.2015.09.005